Multi-physics and Multi-scale Computational Evaluation of the Thrombogenic and Cavitational Potential of a Bileaflet Mechanical Heart Valve

R.K. Nallamothu[1], Yan Li[1], D.R. Rafiroiu[1], V. Díaz-Zuccarini[2], A.J. Narracott[3], P.V. Lawford[3], and D.R. Hose[3]

[1] Electrical Engineering Dep., Technical University, Cluj-Napoca, Romania
[2] Mechanical Engineering Dep., University College, London, United Kingdom
[3] Medical Physics Group, University of Sheffield, Sheffield, United Kingdom

Abstract— **The paper presents a multi-physics and multi-scale modeling approach on the closure dynamics of a bileaflet prosthetic heart valve. The modeling methodology consists of coupling a multi-scale model of the left ventricle contraction to a 3D CFD-FSI model, in order to investigate the closure of a cavity pivot bileaflet valve. The rebound motion of the valve is also modeled. The potential of the valve to generate thrombogenic and cavitation effects are assessed on the basis of the duration for which the blood flow is exposed to elevated wall shear stress, large negative pressure transients and increased flow vorticity. A special attention is given to the flow field in the hinge region of the valve.**

Keywords— **multi-physics, multi-scale, mechanical heart valve, thrombogenicity, cavitation, hinge flow.**

I. Introduction

Cardiovascular engineering is one of the success stories in Bioengineering. A specific example of successful cardiovascular engineering applications is the design analysis of prosthetic heart valves [1]. Although existing techniques, including mechanical heart valves (MHV) and biological valves (BV), have stood the test of time there are still some important issues to solve regarding thrombogenecity of MHVs and life-time duration for biological valves.

Computational Fluid Dynamics (CFD) has emerged as a promising tool, which, alongside experimentation, can yield insights of unprecedented detail into the hemodynamics of prosthetic heart valves. For CFD to realize its full potential, however, it must rely on numerical techniques that can handle the enormous geometrical complexities of prosthetic devices with spatial and temporal resolution sufficiently high to accurately capture all hemodynamically relevant scales of motion [2]. Valve function is driven by interaction between the blood (fluid) and the motion of solid valve structure. In order to examine such systems computationally it is necessary to consider both the solid and the fluid phases simultaneously, which requires a fluid-structure interaction (FSI) analysis. Recent computational models have used both custom and commercial codes such as ANSYS-CFX, ANSYS-Fluent and LS-DYNA.

These have been applied to the study of native mitral [3] and aortic [4] valves and also to determine the fluid dynamic performance of valve prostheses [5].

The effects of the heart, vasculature and the systemic response to the changing physiological environment are often not included within local 3D models of valve function. Multi-physics and multi-scale modeling brings new insight by allowing such interactions to be investigated *in silico*. The use of FSI analyses has highlighted the need for improved and interactive boundary conditions. Solutions include FSI analyses coupled with lumped parameter boundary condition models which can represent biochemical reactions at the cellular level and electro-mechanical events in the heart [6].

Patients with mechanical heart valve implants need to be under long-term anticoagulant therapy in order to minimize problems related to thromboembolic complications [7]. Cavitation bubble development due to the large negative pressure transients on the inflow side of the leaflet edge and their subsequent collapse may contribute to both the platelet activation and the structural damage of the valve [8].

The bileaflet mechanical heart valve (BMHV) has been used for almost two decades and remains the most widely implanted valve design. Like any other mechanical or bio prosthetic heart valve, bileaflet valves are not free from complications. They can still cause major complications including hemolysis, platelet destruction, and thromboembolic events. Investigations have concluded that the stresses imposed on blood by MHVs during the closing phase, in both mitral and aortic position, can initiate hemolysis and the coagulation cascade. Based on their attempts to investigate the leakage, hinge, and near hinge flow fields of different BMHVs [9], manufacturers continuously try to improve the design of their products.

The work presented here is continuation of our previous efforts in building up multi-physics and multi-scale models of the BMHV's fluid mechanics. Our previous work has been done with the purpose of investigating the hemolytic and cavitation potentials of the valves. Focusing on the most critical points of a valve dynamics, the closure and the rebound motion of its leaflets, we were seeking for evidence of high negative pressure transients, high vorticity and high

S. Vlad and R.V. Ciupa (Eds.): MEDITECH 2011, IFMBE Proceedings 36, pp. 298–305, 2011.
www.springerlink.com

wall shear stress values in the hydrodynamic field [10]. Using the same modeling methodology, we are now extending our study to the whole cardiac cycle, focusing not only on the closure of the valve but also on the acceleration phase during systole and on the reverse flow during diastole. Special attention is given to the hinge flow. The valve is considered in mitral position but other studies currently under development are dealing with both the aortic and the mitral valve simultaneously.

II. Computational Model

A. CFD Model

To build up the computer aided design (CAD) model, an explanted 23 mm tissue annulus diameter (TAD) bileaflet mechanical heart valve was laser scanned. The resulted CAD image of the assembled valve is shown in Figure 1.

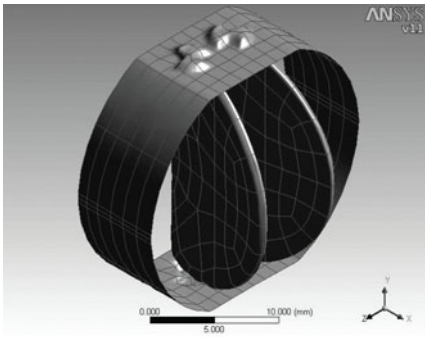

Fig. 1 The CAD image of the scanned valve, consisting of two identical leaflets and the housing

Considering the valve to be mounted in mitral position, the CAD model was completed with two cylindrical chambers representing the atrium and ventricle. The atrial chamber, positioned in the negative OX direction and the ventricular chamber, positioned in the positive OX direction are both 24 mm in length. For saving computational resources, only one quarter of the valve was considered in the 3D model.

Blood was considered as an incompressible Newtonian fluid with density $\rho = 1100\,\mathrm{kg/m^3}$ and dynamic viscosity $\mu = 0.004\,\mathrm{kg/m \cdot s}$. The unsteady flow field inside the valve is described by the 3D equations of continuity and momentum (1), with the boundary conditions suggested by Figure. 2.

$$\rho \frac{\partial \vec{u}}{\partial t} + (\vec{u} \cdot \nabla)\vec{u}\rho = \nabla p + \mu \Delta \vec{u}; \nabla \cdot \vec{u} = 0 \qquad (1)$$

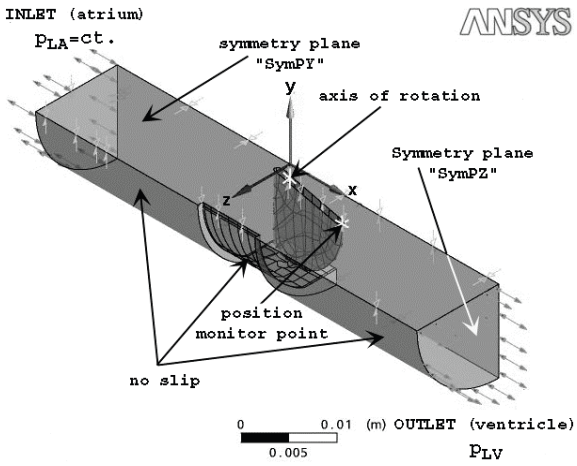

Fig. 2 The overall CAD model and the associated boundary conditions

The fluid-structure interaction model is outlined in Figure 3 and it is based on an explicit incremental method. Each leaflet rotates under the combined effects of hydrodynamic, buoyancy and gravitational forces acting on it. At every time step, the drag $\vec{f}_Q^{\,z}$ and lift $\vec{f}_Q^{\,x}$ force exerted by the flowing fluid on an arbitrary point Q of the leaflet's surface, are reduced to the centroid, G. The total contribution of drag $\vec{F}_G^{\,z}$ and lift $\vec{F}_G^{\,x}$ are added to the difference between the gravitational and buoyancy forces $(\vec{G} - \vec{A})$.

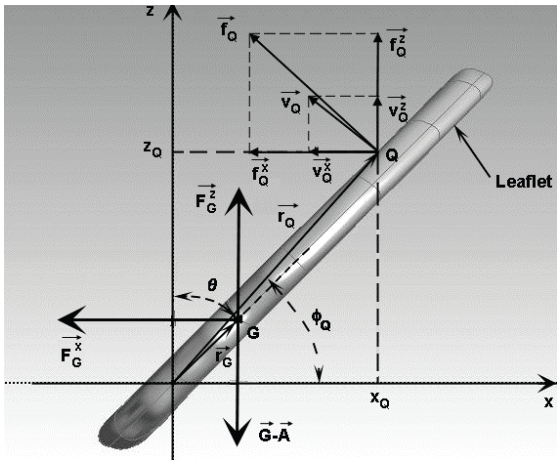

Fig. 3 The fluid-structure interaction model

The condition for the conservation of the kinetic moment is imposed, resulting in the dynamic equation (2) that describes the motion. In equation (2), $d\theta$ represents the leaflet's angular step, dt is the time step, ω_{old} is the angular velocity at the beginning of the current time step and M is

the total moment acted on the leaflet from the external forces. The moment of inertia of each leaflet is $I = 7.21\,\mathrm{g}\cdot\mathrm{mm}^2$.

$$d\theta = \omega_{old}\,dt + \frac{M}{2I}\,dt^2 \tag{2}$$

$$M = r_G\left[F_G^x \sin\theta + \left(F_G^z - G + A\right)\cos\theta\right] \tag{3}$$

As there is speculation that vortexes are likely to occur after the first impact between the leaflet and the valve housing, the rebound motion is also modeled. When, within the current time step, the angular position exceeds $\theta_{reb} = 63.7$ dgrs. corresponding to a minimum distance between the leaflet's periphery and the housing, a virtual torsion spring with constant k is suddenly twisted between the current position and θ_{reb}. The torque exerted by the spring is added to the gravitational force, thus reversing the leaflet's rotation. The dynamic equation changes accordingly:

$$d\theta = \omega_{old}\,dt + \frac{M}{2I}\,dt^2 - k\,\frac{\left(\theta_{old} - \theta_{reb}\right)^2}{2I}\,dt^2 \tag{4}$$

$$\begin{aligned} dx_{new} &= r_Q\left[\cos\left(\varphi_{Q_{old}} + d\theta\right) - \cos\varphi_{Q_{old}}\right] \\ dz_{new} &= r_Q\left[\sin\left(\varphi_{Q_{old}} + d\theta\right) - \sin\varphi_{Q_{old}}\right] \end{aligned} \tag{5}$$

Displacements of every point Q from the surface of the leaflet are calculated as a function of the distance to the center of rotation r_Q, its angular coordinate at the previous time step $\varphi_{Q_{old}}$, and the current angular step $d\theta$, according to equation (5). The current time linear displacements are added to the "old" coordinates and the moving boundary is displaced together with the mesh.

B. *Left Ventricle Model*

For representing the contraction of the left ventricle (LV), a complex boundary condition is used. Figure 4 shows the sub-levels of organization of the ventricle that were taken into consideration. The connection between the LV model and the valve model is also illustrated in figure 4.

A constant pressure source is connected to the atrium via the mitral valve (input model). The blood fills the LV (output model) and ejects a volume of blood into the arterial network via the aortic valve. Contraction in the cardiac muscle is described at a number of levels, starting from the level of the contractile proteins (actin and myosin), following a hierarchical path, from the microscopic level up to the tissue (muscle level) and to the organ level, to finally reach the hemodynamic part of the LV and its arterial load.

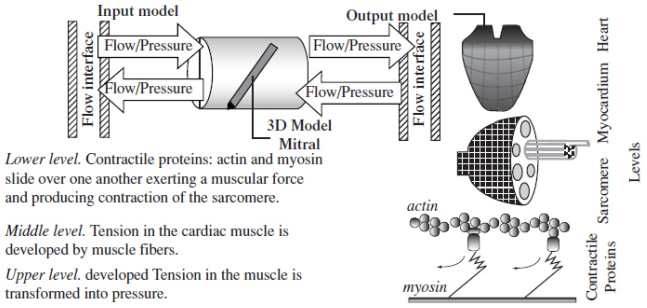

Fig. 4 Representation of the LV model and its different physical scales, coupled to the 3D model of the mitral valve [6].

Complete details of the formulation of the model can be found in [11].

III. Results

The computational model presented in section I has already been used to simulate the valve closure exclusively. The leaflets' movement was separated into two consecutive phases i.e., the *approach* phase and the *rebound* phase. The influences of various parameters of the model, like the intensity of the LV contraction and the resilience coefficient on the cavitation and hemolytic potential of the valve have been investigated [10].

In the current study, we have extended our searching for hemolytic and cavitation evidences to the whole cardiac cycle. Figure 5 shows the pressure and position histories of the valve over a 0.8 s long cardiac cycle. A detail about the bouncing motion of the leaflets is included.

The first to extract from our simulation data was the minimum pressure at the surface of the leaflets. The third panel of figure 5 shows that during the rebound motion, transient negative pressure spikes occur, whilst in the rest of the cardiac cycle the negative pressure values are low. The maximum negative pressure value recorded at the surface of the leaflets during the rebound was of -669.4 mmHg. That is below the vapor pressure of blood of -713 mmHg [12].

This suggests that, under the specifications taken into account in the model and with the inherent influence of the numeric in the results, no cavitation potential exists for this kind of valve. However, it might happen that, at hyperdynamic physiologic states (higher LV pressure rates) [12] and/or grater resilience coefficients [10], the negative pressure spike be greater than the vapor pressure. This demonstrates the potential for cavitation with implanted mechanical valves in vivo.

Yet other mechanisms responsible for cavitation exist. Vortex formations at the atrial side of the valve may contribute to cavitation. In figure 6, the maximum vorticity at

the surface of the leaflets was plotted against time for the entire cardiac cycle. The maximum vorticity occurs during the rebound but still relatively high values are present after the valve closure, at mid-systole and later. That is due to the retrograde flow through the closed valve which may increase the hemolytic potential of the valve.

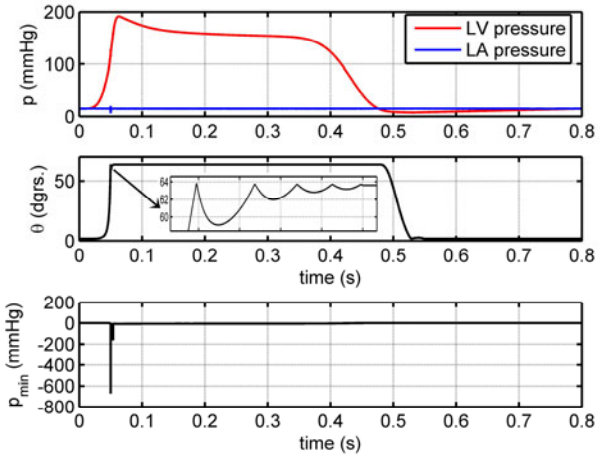

Fig. 5 Total pressure drop on the valve and position history over the entire cardiac cycle, together with the minim pressure at the surface of the leaflets

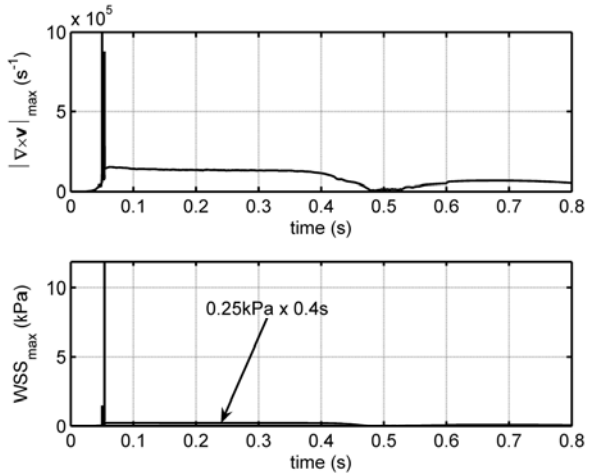

Fig. 6 Maximum vorticity and maximum wall shear stress at the surface of the leaflets vs. time

A relevant indicator of platelet activation is the area under the wall shear stress vs. time curve $\int \tau_{\max}(t)dt$. The values of this integral that exceed $3.5\,\mathrm{Pa}\cdot\mathrm{s}$ are indicators for platelet activation [13]. The second panel of figure 6 shows the maximum wall shear stress values at the surface of the leaflet vs. time. Again, the maximum WSS value (14 kPa) occurs during the rebound but still high values are noticed at mid-systole and later. Using a value of 0.25 kPa for the WSS and 0.4 s for the duration of the stress from the plot, WSS-time product of $100\,\mathrm{Pa}\cdot\mathrm{s}$ is obtained as representative of the area under the curve. The value exceeds the magnitudes of $3.5\,\mathrm{Pa}\cdot\mathrm{s}$ suggested for platelet factor 3 release indicative of platelet activation. This extremely high value is due to the leaking valve during late systole and we have to look for its source in the incomplete closure of the valve and in the hinge flow field.

Numerous researches have sought to characterize the flow field inside the hinge region of BMHVs in an effort to better understand the relationship between hinge design and thromboembolic potential. Most of studies have only captured two-dimensional velocity fields at selected locations [15], [17]. Researchers have resorted to numerical studies to obtain further information on the hinge flow fields. However, the relevance of their results seems to be insufficient, due to "lack of spatial resolution or the use of non-physiologic flow conditions". Simon *et al* [16] have implemented a pseudo multi-scale approach to simulate the three-dimensional physiologic flow in the hinge region of BMHV under aortic conditions.

In the present study, we try to have a preliminary insight into the hinge flow field of a BMHV under mitral conditions, using the multi-physics and multi-scale modeling approach described above. The hinge geometry was characterized using the same nomenclature and methodology as in Simon et al. [16]. The leaflet ear was positioned within the hinge recess such that the gap width (distance between the bottom of the hinge recess and the tip of the leaflet ear, defined as (b-a) in Fig. 7) was approximately 200 μm.

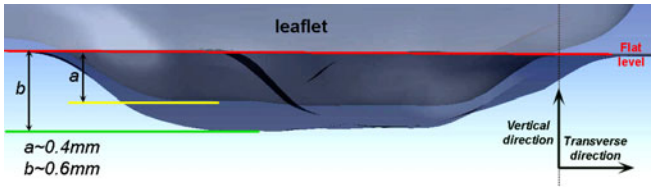

Fig. 7 Side view of the hinge pivot and recess at fully closed position

Figure 8 shows the valvular pressure drop and flow waveforms. The cardiac cycle duration was set to 0.8s which corresponds to a heart rate of 75beat/min. The instances of time corresponding to the beginning of systole, mid-systole, end-systole, mid acceleration and peak-diastole are included. The flow waveform indicates a persistent leakage of the valve after its closure. There are two possible sources for this leakage in our model. One might be a slight deformation of the valve housing either at explantation or

during its preparation for scanning, as the housing and the two leaflets had to be separated. Most certainly, the second source for leakage is the small gap (0.1mm) that had to be foreseen between the leaflet and the hosing in order to model the rebound. That gap allows for the virtual spring (which we have introduced in our model to simulate the rebound) to be compressed by the closing leaflet and to render the elastic deformation energy back to the leaflet, throwing it back. At the end of bouncing, the leaflet settles up at 0.1mm away from the housing, thus maintain this gap all along the systole. A double size gap exists within each hinge, between the leaflet ear and the housing recess. The central gap between the two fully closed leaflets is much smaller. It means that most of the leakage is through the hinges and between the leaflets and the housing.

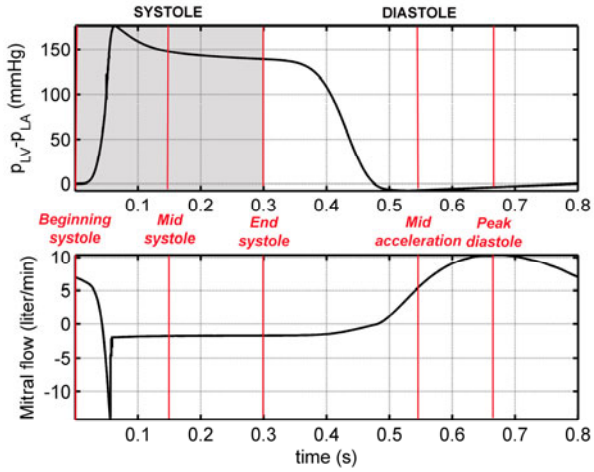

Fig. 8 Valvular pressure drop and flow waveforms

Under these circumstances, which may be thought as inherent somehow, we tried to have a look at the flow fields in the flat level of the hinge, at specific instances during the cardiac cycle (fig. 8 second panel). Figures 9 through 15 illustrate these velocity fields. The direction of the forward flow is from right to left (from left atrium to the left ventricle). Arrows point in the direction of the velocity vector and are colored and sized by velocity magnitude. For a better view of the velocity distribution within the flat level, contour plots were also added to each graph.

Before the onset of the left ventricle contraction (beginning of systole), the valve is still opened and a forward flow passes through the valve. This is the initial state (t=0s) of the valve for the current cardiac cycle. A forward jet at a maximum velocity of 1.26 m/s was found in the central region of the hinge (fig. 9). The same plot shows areas of low

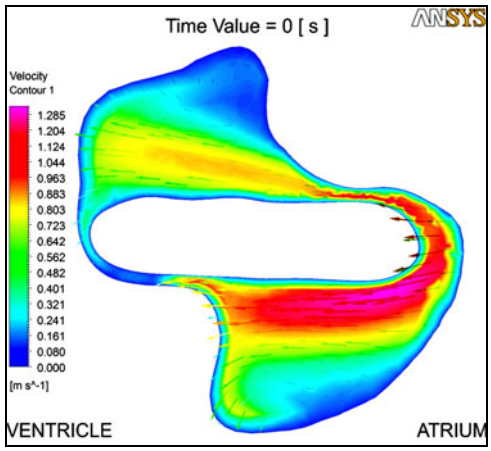

Fig. 9 Flow field at early systole for a 23-mm mitral valve, flat level

velocity in the lower (atrial) and upper (ventricular) corners of the hinge, thus indicating possible vertical flows in those regions.

One hundred and fifty milliseconds later, at mid-systole, the valve is fully closed and a backward leakage jet is observed towards the atrial corner of the hinge (fig. 10). As Leo explains [14], this leakage jet is drawn towards the atrial side of the hinge, at early-systole, by the leaflet. The maximum velocity in the flat-level plane of the hinge is 9.59 m/s. This is much greater than any of the two values given by Leo for the same valve (3.17 m/s at early systole and 2.4 m/s at mid systole).

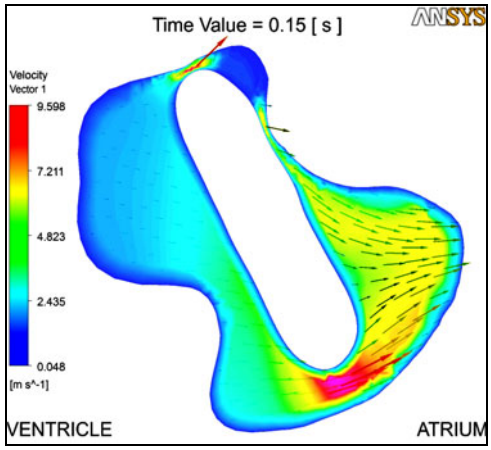

Fig. 10 Flow field at mid-systole for a 23-mm mitral valve, flat level; high backward flow velocities of nearly 10 m/s are present because of the leakage

A similar backward leakage jet was found at the end of systole (fig. 11) but the maxim velocity is a little bit lower (9.37 m/s).

During the diastole, at mid-acceleration, the forward flow recovers, with the same location relative to the leaflet's ear as it was at the end of the previous diastole (fig. 9) but, with a maximum velocity of 0.96 m/s (fig.12) only. The maximum velocity is much lower than the one reported by Leo for the mid diastole. This is the moment when the small flow velocity adjacent to the central forward jet starts generating vortical structures in the corners of the hinge (fig. 13).

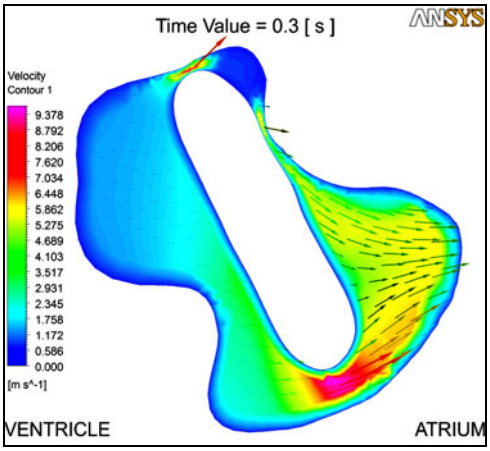

Fig. 11 Flow field at end-systole for a 23-mm mitral valve, flat level; high backward flow velocities of nearly 10 m/s are present because of the leakage.

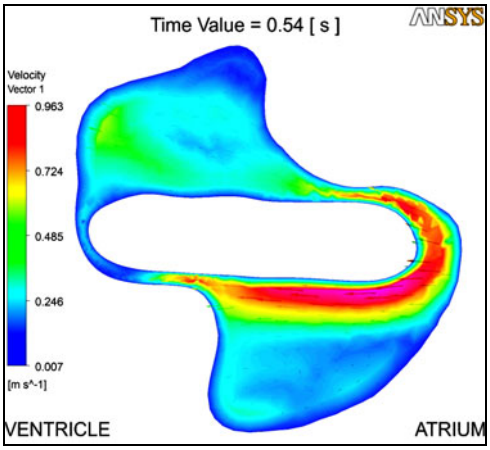

Fig. 12 Flow field at mid-acceleration for a 23-mm mitral valve, flat level

Towards the peak diastole (fig. 14) the forward central jet increases in intensity, the maximum velocity reaching the value of 2.5 m/s. This value is much closer to the one reported by Leo (3.2 m/s). The vortical flow in the corners increases in intensity (fig. 15).

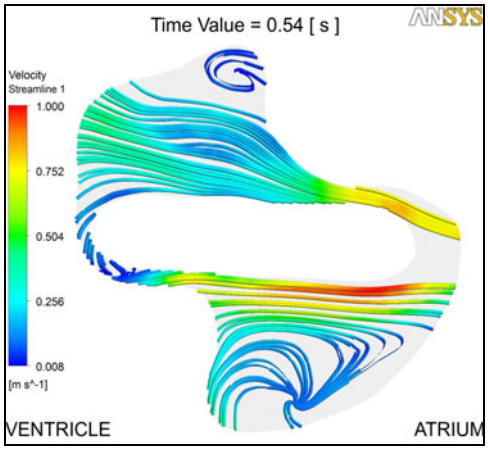

Fig. 13 Streamlines at mid-acceleration for a 23-mm mitral valve, flat level; vortical structures occur in the both the atrial and the ventricular corner of the hinge recess

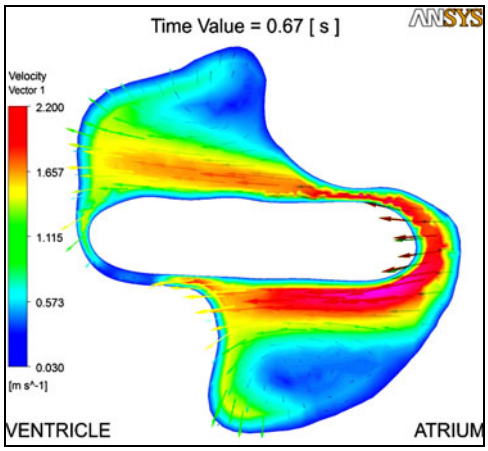

Fig. 14 Flow field at peak-diastole for a 23-mm mitral valve, flat level

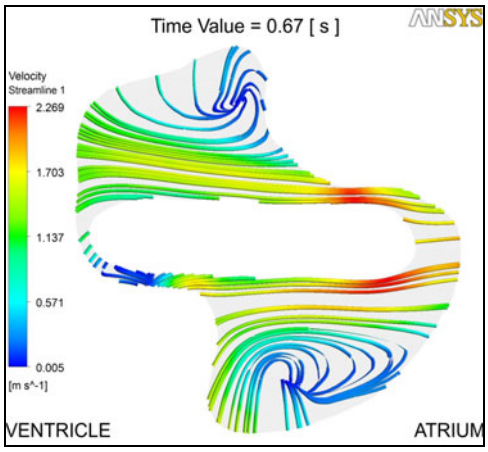

Fig. 15 Streamlines at peak-diastole for a 23-mm mitral valve, flat level; vortical structures develop in the both the atrial and the ventricular corner of the hinge recess

IV. Conclusions

By coupling a multi-scale model of the left ventricle contraction to a three-dimensional CFD-FSI model of a bileaflet mechanical heart valve, we succeeded to draw a picture of the global biomechanics of the valve and to investigate the possible sources for hemolytic and cavitation drawbacks. A special attention was given to the hinge flow field; the results being compared to the experimental ones obtained by other authors for the same type and size of the valve. The general aspects of the simulated hinge flow field were close to the experimental ones, the differences between some of the values being probably caused by some damage that has been brought to the explanted valve and by the rebound model which knowingly leaves a leakage gap between the leaflets and the valve housing.

These results encourage us to continuing our modeling adventure by struggling to get a better representation of the valve geometry and by improving our rebound model such that its influence on the flow field is reduced to the minimum. We are also aware that the two cylindrical chambers representing the atrium and the ventricle are poor approximations of the real geometries of both chambers. Interesting debates about the effects that the actual geometry of the heart might have on the valve functionality are already present in the literature. For example, dependence of the valve-valve interaction on the flow conditions is expected [18]. Therefore, replacing the cylindrical representation of the adjacent chambers of the valves with more realistic geometrical models is also foreseen.

At the same time, the CFD part of the model will be improved by switching from the laminar model that we have used to a turbulent one, thus allowing us to have a better view at the global and local flow fields. We would also be happy to cooperate with our partners from MeDDiCA, particularly with ISS, by comparing their 3D PIV measurements with our numerical simulations.

To the best of our knowledge, the current study is the first numerical modeling insight into the hinge flow field of a bileaflet mechanical heart valve in mitral position. All other studies published so far concern either the aortic position or they are just experimental investigations. We consider MeDDiCA as the best chance we've had to involve ourselves in such an interesting but challenging scientific activity.

Acknowledgment

"This project is funded by the European Commission; Marie Curie Initial Training Networks, FP7-PEOPLE-ITN-MeDDiCA 2008, 238113".

We also take this opportunity to acknowledge the MeDDiCA participants, professors and colleagues for their continuous support.

References

1. Dasi L, Simon H, Sucosky P et al. (2009) Fluid mechanics of artificial heart valves. Clinical and Experimental Pharmacology and Physiology **36**, 225-237
2. Yoganathan A, Chandran K. and Sotiropoulos F. (2005) Flow in Prosthetic Heart Valves: State of-the-Art and Future Directions. Annals of Biomedical Engineering **33**(12) 1689–1694
3. Kunzelman K, Einstein D. and Cochran P (2007) Fluid-structure interaction models of the mitral valve: Function in normal and pathological states. *Phil. Trans. R. Soc. B* **362** 1393–1406
4. Carmody, C., Burriesci, G., Howard, I. and Patterson E (2006) An approach to the simulation of fluid-structure interaction in the aortic valve. *Journal of Biomechanics* **39,** (1) 158-169
5. Watton P, Luo X, et al (2007) Dynamic modeling of prosthetic chorded mitral valves using the immersed boundary method. Journal of Biomechanics **40**(3) 613–626
6. Diaz-Zuccarini V, Hose D, Lawford P, et al (2008) Multiphysics and multiscale simulation: application to a coupled model of the left ventricle and a mechanical heart valve. *International Journal for Multiscale Computational Engineering* **6**(1) 65–76.
7. Johansen, P. (2004) Mechanical heart valve cavitation. Expert Review of Medical Devices **1**(1), 95–104
8. Hwansung L, Yoshiyuki T (2006) Mechanism for cavitation phenomenon in mechanical heart valves. *Journal of Mechanical Science and Technology* **20**(8) 1118–1124
9. Simon H.A. (2005) Influence of the implant location on the hinge and leakage flow fields through bileaflet mechanical heart valves. MS Thesis http://hdl.handle.net/1853/5159
10. Rafiroiu D, Ciupa R (2009) Medical devices design in cardiovascular applications. Current and future trends at Cluj Napoca Technical University. Journal of Nonlinear Optics, Quantum Optics, **39** (2-3) 101-115
11. LeFevre J., LeFevre L. and Couteiro B. (1999) A bond graph model of Chemo-mechanical transduction in the Mammalian left ventricle. *Simulation Practice and Theory* **7**(5–6) 531–552.
12. Dexter EU, Aluri S, Radcliffe RR, et al (1999) In vivo demonstration of cavitation potential of a mechanical heart valve. ASAIO J **45**(5) 436-441
13. Cheng R, Lai Y. and Chandran, K. (2004) Three-dimensional fluid-structure interaction simulation of bileaflet mechanical heart valve flow dynamics. *Ann Biomed. Eng.* **32**(11), 1471–1483.
14. Hwa Liang Leo, (2005) An in vitro investigation of the flow fields through bileaflet and polymeric prosthetic heart valves. PhD Thesis http://hdl.handle.net/1853/11644
15. Ellis JT. and Yoganathan AP. (2000) A comparison of the hinge and near-hinge flow fields of the ST Jude Medical hemodynamic Plus and Regent bileaflet mechanical heart valves, J Thorac Cardiovasc Surg; 119:89-93
16. Simon HA. Ge L. Sotiropoulos F. Yoganathan AP. (2010) Simulation of the three-dimensional hinge flow fields of a bileaflet mechanical heart valve under aortic conditions. Ann Biomed Eng, 38(3): 841-853

17. Simon HA. Leo H-L. Carberry J. Yoganathan AP. (2004) Comparison of the hinge flow fields of two bileaflet mechanical heart valves under aortic and mitral conditions. Ann Biomed Eng, 32(12): 1607-1617
18. Stijnen J.M.A Bogaerds A.C.B de Hart J. Bovendeerd P.H.M. de Mol B.A.J.M. van de Vosse J.M.A. (2009) Computational analysis of ventricular valve-valve interaction: Influence of flow conditions. International Journal of Computational Fluid Dynamics, 23(8): 609-622

Corresponding author:

Rajeev Kumar Nallamothu
Technical University of Cluj-Napoca
26-28 Gerorge Baritiu
Cluj-Napoca
Romania
Rajeev.NALLAMOTHU@et.utcluj.ro